Engineering Transactions, **73**(2): 305–321, 2025, https://doi.org/10.24423/engtrans.3493.2025
Institute of Fundamental Technological Research Polish Academy of Sciences (IPPT PAN)
Université de Lorraine • Poznan University of Technology

Technical Note

Comparative Study of Matrix Methods for Modeling the Dispersive Character of Ultrasonic Guided Waves

Ismaine ZITOUNI*, Hassan RHIMINI, Abdelkerim CHOUAF

Laboratory of Mechanics, Engineering and Innovation,
National School of Electricity and Mechanics, Hassan II University
Casablanca, Morocco; e-mails: h.rhimini@ensem.ac.ma, a.chouaf@ensem.ac.ma

*Corresponding Author e-mail: Ismaine.zitouni.doc20@ensem.ac.ma

This paper presents a comparative study of various matrix methods for obtaining the dispersion curves of ultrasonic guided waves in anisotropic media for both planar and cylindrical geometries. First, the mathematical formulation of the problem is introduced. Then, matrix methods are employed to generate the characteristic dispersion functions, with a particular focus on multilayer structures. To simplify the problem and enhance convergence, the formulation of Lamb modes is separated from that of shear modes. Dispersion curves are then plotted for single and multilayer planar and cylindrical geometries of propagating modes, with each case identifying the different modes obtained and explaining their symmetry characteristics. The dispersion curves are generated using a MATLAB program and compared with two software tools: Disperse Calculator for plates and GUIGUW for cylindrical structures. A perfect match is observed.

A discussion is then presented to highlight the advantages and limitations of the matrix methods, offering reliable insights into which matrix method is most suitable for each type of waveguide and enabling the plotting of convergent curves with minimal computation time.

Keywords: guided waves; dispersion curves; composite; laminate; matrix method; pipeline.

1. Introduction

In recent decades, composite materials have been extensively used in various industries, particularly in the automotive and aerospace sectors. These materials combine the beneficial properties of two or more substances, resulting in enhanced mechanical and thermal characteristics. For instance, graphite-epoxy composites [1, 2] are widely used in the space industry due to their high structural rigidity, reduced thermal distortion, and low weight. However, these composites are prone to damage and degradation of interlayer adhesion due to cyclic loading during operation and exposure to environmental factors. Furthermore, poor adhesion between the fiber and matrix can result in the formation

of defects, which are, in some cases, challenging to detect. Non-destructive testing (NDT) using ultrasonic guided waves (UGW) offers an effective means of identifying such defects. UGW generates vibrations throughout the material being inspected, and when these waves encounter defects, they are reflected and detected by sensors. By analyzing the sensor signals, information regarding the position, depth, and size of the defect can be determined. However, effective use of UGW in an inspection system requires an understanding of dispersion curves, which describe the frequencies and velocities of waves propagating through the material. Significant research has been devoted to calculating and plotting these dispersion curves of UGW in composite structures. Numerous methods and techniques have been developed for this purpose. The transfer matrix method (TMM) [3], for instance, was introduced to plot Lamb wave dispersion curves for multilayer anisotropic materials, with Nayfeh [4] extending this approach to address shear horizontal (SH) waves. Despite its straightforward formulation, TMM has limitations, particularly at high frequencies and for thick layers, leading to instabilities in the results.

Datta [5] noted that under these conditions, the transfer matrix presents singular values due to its exponential dependence. To address these challenges, the stiffness matrix method (SMM) [5, 6] was developed. This approach reformulates the problem by consolidating the stresses of a layer into a single vector, resulting in a stiffness matrix that overcomes the singularities observed with TMM. However, as the number of layers increases, both methods become insufficient. The global matrix method (GMM) was subsequently introduced to improve the accuracy of dispersion curve calculations. Recognizing the potential of GMM, Pavlakovic *et al.* [7] developed the industrial software Disperse, which has become a leading tool in ultrasonic NDT and is widely endorsed by researchers. Nevertheless, Disperse encounters limitations when dealing with laminates exceeding several hundred layers.

Kamal *et al.* [6] and Monnier [8] proposed the equivalent matrix method, which involves calculating an equivalent behavior matrix for the entire laminate. While this method achieves accuracy at low frequencies for the first symmetric (S0) and asymmetric (A0) modes in periodic stacks (0° and 90°), its applicability is limited to these conditions. Other methods, such as the semi-analytical finite elements (SAFE) method [9, 10], the spectral method [11–13], and the Legendre polynomial-based method [14], have also been introduced. These numerical approaches offer significant advantages in terms of computational efficiency and simplicity of implementation. In addition to Disperse, recent years have seen the emergence of free software and applications for calculating the dispersion properties of UGW in various waveguides. Notable examples include the graphical user interface for guided ultrasonic waves (GUIGUW) [15], which uses the SAFE method, and the dispersion calculator (DC) software developed

by HUBER [16], based on SMM. These tools are capable of modeling UGW propagation in layered composites comprising several hundred plies.

The objective of this work is to model the behavior of ultrasonic guided waves in laminated composites using the analytical matrix methods of SMM and TMM. To achieve this, the formulations for Lamb waves and transverse shear waves were separated, enabling improved accuracy and reduced instability. The proposed approach was applied to monolayer, bilayer, and trilayer structures with antisymmetric stacking. For each case, the different modes obtained and their symmetry characteristics were identified and analyzed. The results were compared with those produced by two software tools: the dispersion calculator, which employs the SMM method [16], and GUIGUW, which uses the SAFE method. A perfect agreement was observed between the results of the two matrix methods and the software outputs. Building on these results, a comparative study was conducted to evaluate the performance of the matrix methods in terms of computation time and convergence across low and high-frequency ranges. The SMM method demonstrated its ability to generate dispersion curves across the entire frequency range, unlike TMM, which faces ill-conditioning issues at high frequencies. Furthermore, SMM was found to model the dispersive behavior of UGW more efficiently than TMM, offering faster computation times. These findings provide reliable insights into the suitability of each matrix method for different types of waveguides. They also demonstrate which method is more effective for plotting convergent dispersion curves with minimal computation time.

2. Theoretical formulation

We consider the UGW propagation in a laminated composite with N stress-free layers, each having a thickness h in the x_3 direction. The structure is assumed to be unlimited in both the x_1 and x_2 directions (Fig. 1). We use two coordinate systems: (x_1, x_2, x_3) is a reference Cartesian coordinate system and (x_1', x_2', x_3') is a global Cartesian coordinate system linked to the position of the fibers, where ϕ is the angle describing the rotation between the two coordinate systems.

The displacement components can be written in the reference Cartesian coordinate system as [3–5]:

$$\left(u_1^{(l)}, u_2^{(l)}, u_3^{(l)}\right) = \sum_{q=1}^{6} \left(1, V_q^{(l)}, W_q^{(l)}\right) U_{1q}^{(l)} e^{ik(x_1+\alpha_q^{(l)}x_3-ct)}, \tag{2.1}$$

where $u_j^{(l)}$ $(j = 1, 2, 3)$ are the components of the displacements of layer l along the x_j directions, q is a summation index, k is the wave number along the

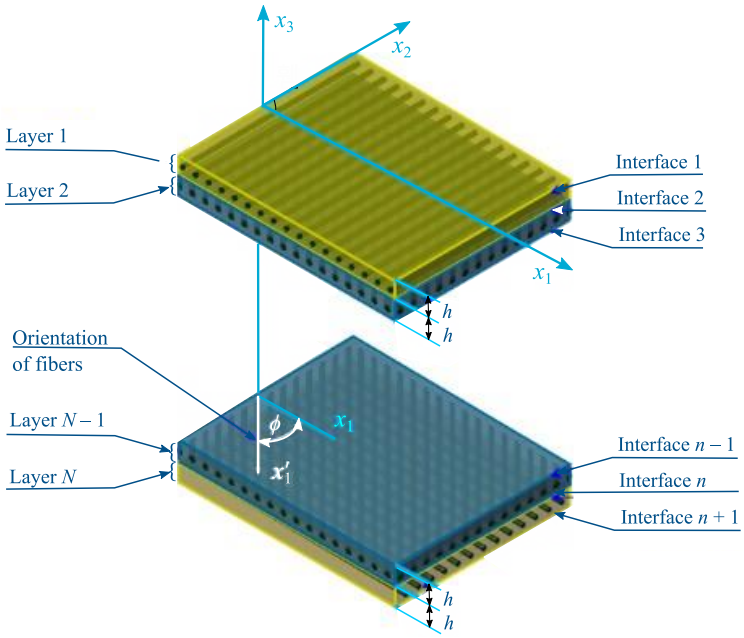

FIG. 1. N-layer planar laminate composite.

propagation direction x_1, c is the phase velocity and the index l represents the layer number, varying from I to N, and i is the imaginary entity ($i^2 = -1$), $V_q^{(l)}$ and $W_q^{(l)}$ are the amplitude ratios expressed as follows:

$$V_q^{(l)} = \frac{K_{11}^{(l)}\left(\alpha_q^{(l)}\right) K_{23}^{(l)}\left(\alpha_q^{(l)}\right) - K_{13}^{(l)}\left(\alpha_q^{(l)}\right) K_{12}^{(l)}\left(\alpha_q^{(l)}\right)}{K_{13}^{(l)}\left(\alpha_q^{(l)}\right) K_{22}^{(l)}\left(\alpha_q^{(l)}\right) - K_{12}^{(l)}\left(\alpha_q^{(l)}\right) K_{23}^{(l)}\left(\alpha_q^{(l)}\right)},$$

$$W_q^{(l)} = \frac{K_{11}^{(l)}\left(\alpha_q^{(l)}\right) K_{23}^{(l)}\left(\alpha_q^{(l)}\right) - K_{13}^{(l)}\left(\alpha_q^{(l)}\right) K_{12}^{(l)}\left(\alpha_q^{(l)}\right)}{K_{12}^{(l)}\left(\alpha_q^{(l)}\right) K_{33}^{(l)}\left(\alpha_q^{(l)}\right) - K_{23}^{(l)}\left(\alpha_q^{(l)}\right) K_{13}^{(l)}\left(\alpha_q^{(l)}\right)}, \tag{2.2}$$

where K_{ij} are the coefficients described in [3], and they depend on the elasticity constants, density and phase velocity, $U_{1q}^{(l)}$ are the displacement amplitudes.

Using Hooke's law and the strain-displacement relationship, the stresses associated with these displacements can be expressed as follows:

$$\left(\sigma_{33}^{(l)}, \sigma_{23}^{(l)}, \sigma_{13}^{(l)}\right) = \sum_{q=1}^{6} \left(D_{1q}^{(l)}, D_{2q}^{(l)}, D_{3q}^{(l)}\right) U_{1q}^{(l)} e^{ik(x_1 + \alpha_q^{(l)} x_3 - ct)}, \tag{2.3}$$

where $D_{iq}^{(l)}$ represent the stress amplitudes, which can be written as follows:

$$
\begin{aligned}
D_{1q}^{(l)} &= C_{13}^{(l)} + \alpha_q^{(l)} C_{35}^{(l)} + \left(C_{36}^{(l)} + \alpha_q^{(l)} C_{34}^{(l)}\right) V_q^{(l)} + \left(C_{35}^{(l)} + \alpha_q^{(l)} C_{33}^{(l)}\right) W_q^{(l)}, \\
D_{2q}^{(l)} &= C_{15}^{(l)} + \alpha_q^{(l)} C_{55}^{(l)} + \left(C_{56}^{(l)} + \alpha_q^{(l)} C_{45}^{(l)}\right) V_q^{(l)} + \left(C_{55}^{(l)} + \alpha_q^{(l)} C_{35}^{(l)}\right) W_q^{(l)}, \\
D_{3q}^{(l)} &= C_{14}^{(l)} + \alpha_q^{(l)} C_{45}^{(l)} + \left(C_{46}^{(l)} + \alpha_q^{(l)} C_{44}^{(l)}\right) V_q^{(l)} + \left(C_{45}^{(l)} + \alpha_q^{(l)} C_{34}^{(l)}\right) W_q^{(l)},
\end{aligned} \tag{2.4}
$$

where C_{ij} are the elasticity constants that depend on the angle ϕ.

In order to obtain the dispersion equations for multilayer waveguides, we need to use matrix methods to describe the continuity of displacements and stresses between layers. In the following sections, we will describe the development of the transfer matrix method and the stiffness matrix method.

3. Transfer matrix method (TMM)

TMM involves expressing the displacements and stresses at the laminate's upper interface in terms of those of the lower interface, while respecting the continuity of displacements and stresses between layers. To achieve this, the displacements (Eq. (2.1)) and stresses (Eq. (2.3)) are grouped into a single vector, called the state vector $H^{(l)}$. This vector depends on the displacement amplitudes $U_{1q}^{(l)}$ and is defined as:

$$
\{H\}^{(l)} = \left\{u_1^{(l)}, u_2^{(l)}, u_3^{(l)}, \sigma_{33}^{(l)}, \sigma_{23}^{(l)}, \sigma_{13}^{(l)}\right\}. \tag{3.1}
$$

By expressing the state vectors on both sides of the same layer, we obtain a relationship that combines the components of displacements and stresses on both sides of the same layer. The resulting matrix is called the transfer matrix $A^{(l)}$. To calculate this laminate transfer matrix, all we need to do is to multiply the transfer matrices for each layer $A = A^{(I)} A^{(II)} ... A^{(N)}$:

$$
\begin{aligned}
\{H\}_{(6,1)}^{(l)} &= [X]_{(6,6)}^{(l)} \{U_{jq}\}_{(6,1)}^{(l)}, \\
\{H\}_{(6,1)}^{1} &= [A]_{6,6} \{H\}_{(6,1)}^{n+1}.
\end{aligned} \tag{3.2}
$$

With the expressions of the matrix $[X]_{(6,6)}^{(l)}$ and the transfer matrix $[A]_{(6,6)}^{(l)}$ written as:

(3.3)
$$[X]^{(l)}_{(6,6)} = \begin{bmatrix} 1 & 1 & 1 & 1 & 1 & 1 \\ V_1^{(l)} & V_1^{(l)} & V_3^{(l)} & V_3^{(l)} & V_5^{(l)} & V_5^{(l)} \\ W_1^{(l)} & -W_1^{(l)} & W_3^{(l)} & -W_3^{(l)} & W_5^{(l)} & -W_5^{(l)} \\ D_{11}^{(l)} & D_{11}^{(l)} & D_{13}^{(l)} & D_{13}^{(l)} & D_{15}^{(l)} & D_{15}^{(l)} \\ D_{21}^{(l)} & -D_{21}^{(l)} & D_{23}^{(l)} & -D_{23}^{(l)} & D_{25}^{(l)} & -D_{25}^{(l)} \\ D_{31}^{(l)} & -D_{31}^{(l)} & D_{33}^{(l)} & -D_{33}^{(l)} & D_{35}^{(l)} & -D_{35}^{(l)} \end{bmatrix},$$

$$[A]^{(l)}_{(6,6)} = [X]^{(l)}_{(6,6)} \begin{bmatrix} e^{ik\alpha_1^{(l)}h} & 0 & 0 & 0 & 0 & 0 \\ 0 & e^{ik\alpha_2^{(l)}h} & 0 & 0 & 0 & 0 \\ 0 & 0 & e^{ik\alpha_3^{(l)}h} & 0 & 0 & 0 \\ 0 & 0 & 0 & e^{ik\alpha_4^{(l)}h} & 0 & 0 \\ 0 & 0 & 0 & 0 & e^{ik\alpha_5^{(l)}h} & 0 \\ 0 & 0 & 0 & 0 & 0 & e^{ik\alpha_6^{(l)}h} \end{bmatrix} [X]^{-1\,(l)}_{(6,6)},$$

the boundary conditions of a stress-free laminate result in the cancellation of stresses at the top and bottom interfaces, providing the following:

(3.4)
$$\begin{vmatrix} A_{41} & A_{42} & A_{43} \\ A_{51} & A_{52} & A_{53} \\ A_{61} & A_{62} & A_{63} \end{vmatrix} = 0.$$

4. Stiffness matrix method (SMM)

In contrast to the TMM, the SMM method involves grouping the stresses at the upper and lower interfaces of a layer into a single vector and expressing them in terms of their associated displacements. The result is a layer stiffness matrix, as described by equation:

(4.1)
$$\begin{Bmatrix} \{\sigma\}_1 \\ \{\sigma\}_2 \end{Bmatrix}_{(6,1)} = [S]^{(l)}_{(6,6)} \begin{Bmatrix} \{u\}_1 \\ \{u\}_2 \end{Bmatrix}_{(6,1)},$$

where $[S]^{l}_{(6,6)}$ is the stiffness matrix of the layer described in [5], and it depends on the parameters $D_{jq}^{(l)}$, $V_q^{(l)}$, $W_q^{(l)}$ and $\alpha_q^{(l)}$.

The expression for the stiffness matrix $[S]^{(l)}_{(6,6)}$ is in the form of:

$$(4.2)\quad [S]^{(l)}_{(6,6)} = \begin{bmatrix} D^{(l)}_{11} & D^{(l)}_{13} & D^{(l)}_{15} & D^{(l)}_{11}a^* & D^{(l)}_{13}b^* & D^{(l)}_{15}c^* \\ D^{(l)}_{21} & D^{(l)}_{23} & D^{(l)}_{25} & -D^{(l)}_{21}a^* & -D^{(l)}_{23}b^* & -D^{(l)}_{25}c^* \\ D^{(l)}_{31} & D^{(l)}_{33} & D^{(l)}_{35} & -D^{(l)}_{31}a^* & -D^{(l)}_{33}b^* & -D^{(l)}_{35}c^* \\ D^{(l)}_{11}a^* & D^{(l)}_{13}b^* & D^{(l)}_{15}c^* & D^{(l)}_{11} & D^{(l)}_{13} & D^{(l)}_{15} \\ D^{(l)}_{21}a^* & D^{(l)}_{23}b^* & D^{(l)}_{25}c^* & -D^{(l)}_{21} & -D^{(l)}_{23} & -D^{(l)}_{25} \\ D^{(l)}_{31}a^* & D^{(l)}_{33}b^* & D^{(l)}_{35}c^* & -D^{(l)}_{31} & -D^{(l)}_{33} & -D^{(l)}_{35} \end{bmatrix}$$

$$\cdot \begin{bmatrix} 1 & 1 & 1 & a^* & b^* & c^* \\ V^{(l)}_1 & V^{(l)}_3 & V^{(l)}_5 & V^{(l)}_1 a^* & V^{(l)}_3 b^* & V^{(l)}_5 c^* \\ W^{(l)}_1 & W^{(l)}_3 & W^{(l)}_5 & -W^{(l)}_1 a^* & -W^{(l)}_3 b^* & -W^{(l)}_5 c^* \\ a^* & b^* & c^* & 1 & 1 & 1 \\ V^{(l)}_1 a^* & V^{(l)}_3 b^* & V^{(l)}_5 c^* & V^{(l)}_1 & V^{(l)}_3 & V^{(l)}_5 \\ W^{(l)}_1 a^* & W^{(l)}_3 b^* & W^{(l)}_5 c^* & -W^{(l)}_1 & -W^{(l)}_3 & -W^{(l)}_5 \end{bmatrix}^{-1},$$

where

$$a^* = e^{ik\alpha^{(l)}_1 h}, \qquad b^* = e^{ik\alpha^{(l)}_3 h}, \qquad c^* = e^{ik\alpha^{(l)}_5 h}.$$

Next, the laminate's global stiffness matrix is obtained using an interlayer recursive algorithm based on the equality of interlayer stresses. The result is a system that links the stresses on the top and bottom faces of the laminate. Assuming zero stresses at interfaces 1 and $n+1$ (see Fig. 1), the characteristic dispersion equation of the laminate is obtained by considering the cancellation of the determinant of the global stiffness matrix.

5. Numerical results and discussion

In this section, we will plot the dispersion curves of a graphite-epoxy unidirectional fiber laminate composite with a thickness of $h = 4$ mm and a density of $\rho = 1.61$ g/cm^3. The values of the elastic constants of this material are given in Table 1 and are expressed in GPa.

Table 1. Elasticity constants of the graphite-epoxy composite plate [5].

C_{11}	C_{22}	C_{33}	C_{12}	C_{13}	C_{23}	C_{44}	C_{55}	C_{66}
162	17	17	11.8	11.8	8.2	4.4	8	8

To plot the dispersion of this material, we developed a MATLAB program that plots these curves in the (frequency, wavenumber) plane. The frequency range used is $f = 10 : 50 : 6 \cdot 10^6$ Hz and the wavenumber range is $k = 10^{-5} : 100 : 12\,000$ m^{-1}. We used the bisection method as the algorithm for finding the zeros of the characteristic function [19, 20]. We compare our results with those obtained using the DC software [16].

The algorithm used is shown in Fig. 2.

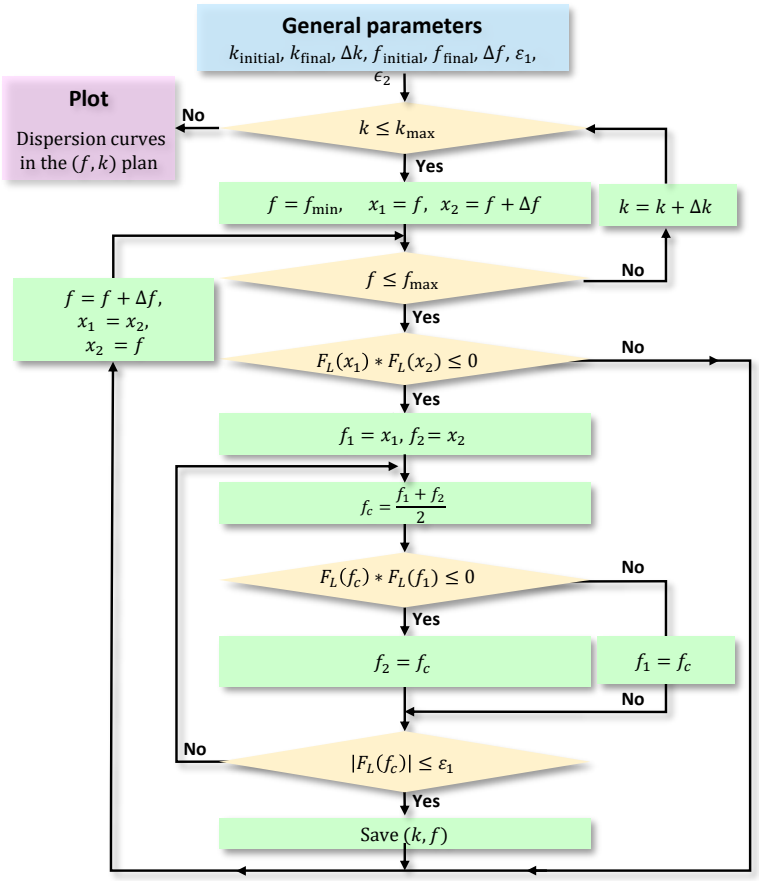

FIG. 2. Bisection method algorithm.

5.1. Case of a composite layer

In this section, we consider the case of a monolayer laminated composite structure made of unidirectional graphite fiber. For angles $\phi = 0°$ and $90°$, the horizontal transverse modes (SH_n) are uncoupled from the Lamb modes, allowing for separate treatment of the two wave types. In addition, for each

wave type, we have symmetric (S_n et SHS_n) and antisymmetric (A_n et SHA_n) modes. We have developed an efficient procedure [11, 12] for classifying the results obtained by exploiting the symmetry and antisymmetry properties of Lamb and SH modes.

Figure 3 shows the dispersion curves of the Lamb and SH modes of the graphite-epoxy composite in the (fV_p) plane for fiber orientations of 0° and 90°. The curves obtained using the SMM and TMM methods are compared with those obtained using the DC software. The superposition of the curves demonstrates the accuracy of the solutions obtained at low frequencies ($0 < f \leq 600$ kHz). At high frequencies ($f > 600$ kHz), the TMM method fails to plot dispersion curves, due to instabilities in the method. This instability is due to the singular values of the transfer matrix. Indeed, the components of matrix $[A]$ are expressed as a function of $e^{-i\mathbf{k}\alpha_q x_3}$. For large values of frequency and wavenumber, the exponential terms tend towards zero, making the transfer matrix highly singular. Because of this singularity, our MATLAB program for finding solutions to the dispersion equations enters an infinite loop and fails to provide reliable solutions.

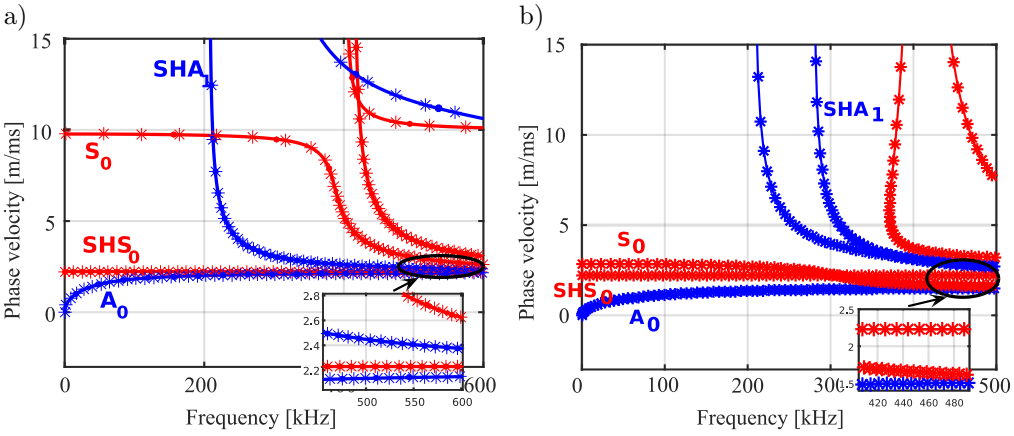

FIG. 3. Dispersion curves of a monolayer graphite-epoxy composite plate for: a) fiber orientations 0° and b) 90°. Solid lines – DC software; points – TMM; stars – SMM.

The SMM, which is considered to be numerically stable, made it possible to obtain dispersion curves for higher frequencies. This is why SMM [5, 6, 17, 18] is so useful for obtaining dispersion curves for monolayer composites.

Table 2 plots the squared errors Er_1 (between DC software and TMM method frequencies) and Er_2 (between DC software and SMM method frequencies) at a frequency of $f = 110$ kHz for the two treated monolayer plates. We considered the first three modes (S_0, A_0 and SHS_0). An error of the order of 10^{-7} was obtained for both methods, demonstrating the accuracy of the results obtained.

TABLE 2. Phase velocity [m/ms] of the methods used for monolayer plates at frequency of $f = 110$ kHz. $Er_1 = \sqrt{(V_{DC} - V_{TMM})^2}$ et $Er_2 = \sqrt{(V_{DC} - V_{SMM})^2}$.

Waveguides	Modes	Er_1	Er_2
Composite plate 0°	S_0	$9.757\ 10^{-7}$	$7.623\ 10^{-7}$
	A_0	$9.517\ 10^{-7}$	$1.869\ 10^{-7}$
	SHS_0	$2.229\ 10^{-7}$	$2.001\ 10^{-8}$
Composite plate 90°	S_0	$2.819\ 10^{-7}$	$5.211\ 10^{-7}$
	A_0	$8.778\ 10^{-7}$	$1.178\ 10^{-7}$
	SHS_0	$3.669\ 10^{-7}$	$2.229\ 10^{-8}$

5.2. Composite planar laminates

In this subsection, we will study the following laminates: a 4 mm-thick bilayer laminate composite with the fiber orientations [0° 90°] for each layer, and two 3 mm-thick three-layer laminate composite plates, with fiber orientations [0° 90° 90°] and [0° 0° 90°] for each layer, respectively. The stacks of the three-layer structures are arranged antisymmetrically with respect to the middle layer. TMM and SMM methods will be used to plot dispersion curves for these three cases. The results will be compared with those from the DC software for validation.

Figure 4 shows the dispersion curves of the three laminated composites. Considering the antisymmetrical arrangement of the layers in three previous cases with respect to the median axis, the modes present in these structures do not resemble those mentioned earlier. Instead, we find modes (M_n), which we call pseudo-Lamb modes, and modes (M_n), which we call pseudo-transverse modes. Both matrix methods were able to model UGW dispersion for the two and three-layer composite laminates. Since the laminate representations are obtained by combinations of angle $\phi = 0°$ and 90°, the wave formulations can be separated [3, 4]. Indeed, in this case, the displacements that define the propagation of Lamb pseudo-modes will be dependent on four constants (C_{11}, C_{22}, C_{33}, and C_{44}) and those of transverse pseudo-modes on two constants (C_{55} and C_{66}). This dependence affects the size of the matrix and, consequently, the dispersion relationships. We then find more simplified formulations in both methods (SMM and TMM). For TMM, instabilities are almost no longer present in the M_n modes (solutions obtained throughout the frequency range), but they remain in the M_n modes (solution valid for $0 < f \leq 700$ kHz). Note that this simplification cannot be implemented in cases where Lamb modes are coupled with SH modes (such as for fiber orientations different from 0° and 90°) [6, 17].

In the following, we will consider a cylindrical waveguide and carry out a comparative study between matrix methods for plotting the dispersion curves of this type of structure.

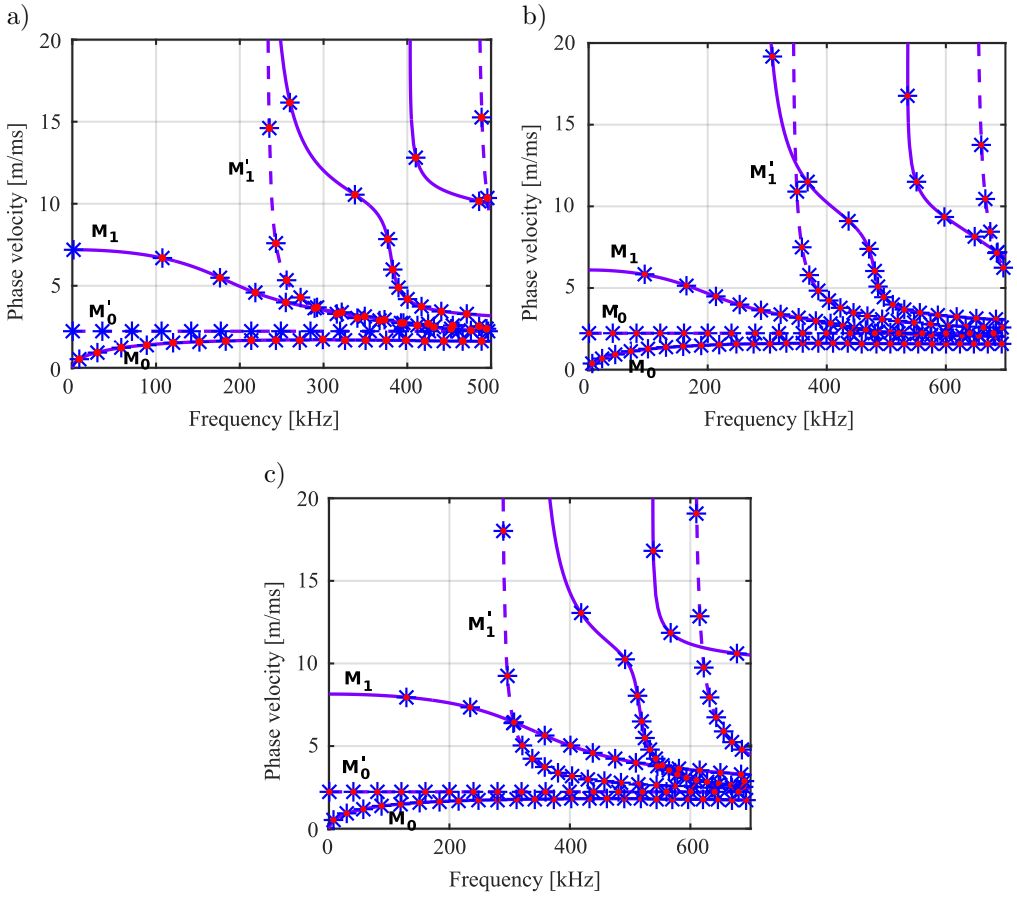

FIG. 4. Dispersion curves: a) a 4 mm two-layer plate [0° 90°], b) a 3 mm three-layer plate of the epoxy graphite composite for representations [0° 90° 90°], and c) [0° 0°90°]. Solid lines – DC software; points – TMM; stars – SMM.

5.3. Composite pipeline

We now consider UGW propagation in a homogeneous multilayer cylindrical waveguide with N layers, as shown in Fig. 5.

The displacement field of a harmonic wave [21] is written in cylindrical coordinates as follows:

$$
\begin{aligned}
u_r &= U_1^m(r)\cos(m\theta)\, e^{i(k_z^m z - wt)},\\
u_\theta &= U_2^m(r)\sin(m\theta)\, e^{i(k_z^m z - wt)},\\
u_z &= U_3^m(r)\cos(m\theta)\, e^{i(k_z^m z - wt)},
\end{aligned}
\tag{5.1}
$$

where U_1^m, U_2^m, U_3^m represent the radial components and m is a positive number representing the order of the circumferential mode.

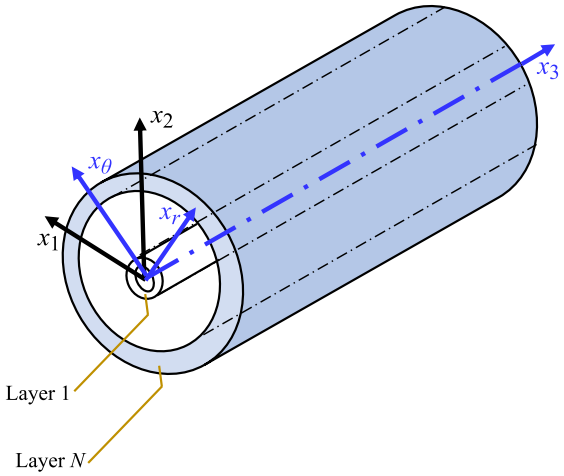

FIG. 5. N-layer cylindrical waveguide; (x_1, x_2, x_3) – Cartesian coordinate system, (x_r, x_θ, x_3) – cylindrical coordinate system.

Cylindrical structures are characterized by longitudinal L(0, n) modes, which propagate along the waveguide and torsional T(0, n) modes, which propagate around the circumference. Due to the curvature of the pipeline, the symmetrical character of the modes is no longer present. Here, n represents the index of the mode's appearance.

We will study three cases: two monolayer graphite-epoxy composite pipelines with fiber directions 0° and 90°, and a bilayer pipeline with orientations [0° 90°]. In the case of monolayer pipelines, the longitudinal and torsional modes are uncoupled. However, in the case of bilayer pipelines, the two modes are coupled together, symbolized as LT(0, n).

Figure 6 shows the dispersion curves of both monolayer and bilayer graphite-epoxy composite pipelines. Figure 6a shows the curves for layer with a fiber orientation of 0° and Fig. 6b those for a fiber orientation of 90°. We chose to compare our results with the GUIGUW interface software, specializing in modeling UGW propagation in cylindrical structures [15]. In both cases, we obtained curves in perfect agreement with the GUIGUW software. The error is estimated to be 10^{-7} between the solutions obtained by matrix methods and those from the software. The modes present in both pipelines are the longitudinal L(0, n) and torsional T(0, n) modes. Figure 6c shows the dispersion curves for the bilayer pipeline [0° 90°]. In this type of structure, the modes are coupled, symbolized as LT(0, n). The results obtained are in perfect agreement with those of the GUIGUW software, with an error of the order of 10^{-7}.

The TMM method encounters the same problem as the frequency increases, the program enters infinite loops caused by matrix ill-conditioning. SMM, on the

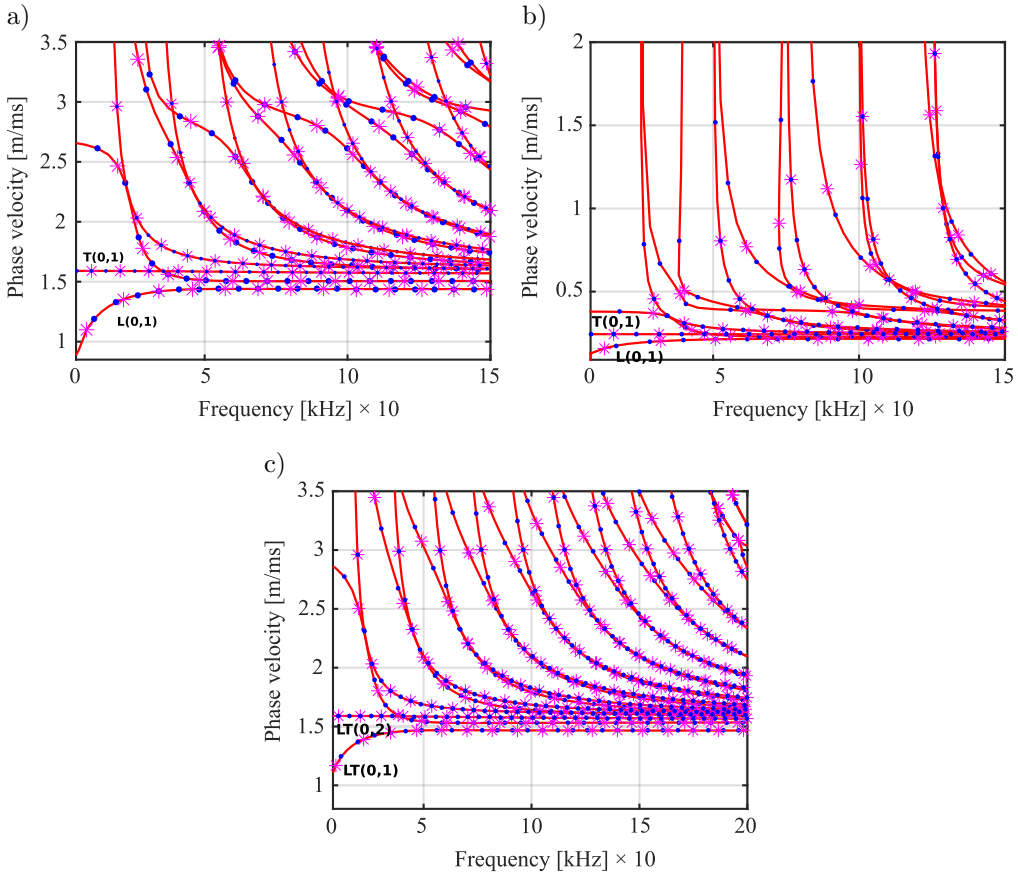

FIG. 6. Dispersion curves: a) a 0°, b) 90° fiber direction composite pipeline, and c) a bilayer pipeline [0° 90°]. Solid lines – GUIGIW software; points – TMM; stars – SMM.

other hand, does not encounter this problem and allows the dispersion curves to be plotted throughout the chosen frequency range.

6. Discussion

We now wish to compare the matrix methods discussed in this paper. The criterion chosen for comparison is calculation time. Table 3 shows the computation times of the TMM and SMM methods for the different waveguides treated.

From the results in Table 3, we can see that the TMM and SMM methods were able to determine the dispersion curves of the various waveguides across the chosen range of wavenumbers, considering only low frequencies ($f < 500$ kHz) to avoid the TMM entering infinite loops. We note that the computation times for plotting SH modes (as well as torsional modes for pipelines) are quite low compa-

Table 3. Computation times for the matrix methods used across a range of wavenumbers $k = 10^{-5} : 100 : 12\,000\ \mathrm{m}^{-1}$.

Waveguide	Modes	TMM	SMM
Monolayer plate 0°	Lamb modes	3265	1050
	SH modes	1802	1762
Bilayer laminate [0° 90°]	Lamb modes	6193	4003
	SH modes	2061	2042
Three-layer flat laminate [0° 90° 90°]	Lamb modes	11 523	7448
	SH modes	5012	4821
Three-layer flat laminate [0° 90°]	Lamb modes	12 321	8617
	SH modes	5047	4997
Monolayer pipeline 0°	Longitudinal modes	9162	7395
	Torsional modes	5293	3854
Bilayer pipeline [0° 90°]	Longitudinal modes	–	20 981
	Torsional modes	13 892	10 253

red to those for Lamb modes (as well as longitudinal modes for pipelines). This is normal, as the anisotropic formulation in planar waveguide of Lamb modes requires two displacements (u_1 and u_3), whereas SH modes are only described by the u_2 displacement (the same for cylindrical formulation). We also observe that as the number of layers increases, so does the computation time, which is anticipated as the formulation becomes denser and more complex. The SMM method plots dispersion curves faster than the TMM for the different types of structure considered. The results in Table 3 were obtained on an Intel(R) Core(TM) i5-6300U CPU @ 2.40 GHz 2.50 GHz with 8 GB RAM on the reference machine.

7. Conclusion

Matrix methods provide a highly efficient approach for plotting the dispersion curves of multilayer composites in both planar and cylindrical geometries. In this study, we focused on the TMM, which exhibited instabilities at high frequencies and large wavenumbers. To address these issues, we proposed a simplified formulation for cases where the modes are uncoupled. This approach significantly reduced the size of the matrix, thereby minimizing the occurrence of singular values. We also investigated the SMM, which avoids the inherent weaknesses of TMM but remains influenced by the number of layers and the thickness of the structure being analyzed. Similarly, a simplified formulation was applied to uncoupled modes, which strengthened the stiffness matrix and reduced these de-

pendencies. The reliability of the results was validated through comparisons with DC software for planar geometries and GUIGUW software for cylindrical geometries. Additionally, we studied the influence of fiber orientations on the types of modes generated. These findings encourage further investigation into the effects of ply orientation and layer thickness on matrix conditioning. Future work will focus on developing techniques to mitigate ill-conditioning and achieve greater convergence, thereby improving the robustness and applicability of these matrix methods.

Declaration

Conflict of interest

On behalf of all the authors, the corresponding author declares that there is no conflict of interest in the publication of this paper.

References

1. Yao D., Zheng J., Jin L., Meng X., Zhan Z., Fan R., Ming P., Effect of surface oxidation on the interfacial and mechanical properties in graphite/epoxy composites composite bipolar plates, *Chinese Chemical Letters*, **35**(11): 109382, 2023, https://doi.org/10.1016/j.cclet.2023.109382.

2. Boushab D., Ouidadi H., Mote A., Priddy M., Kundu S., Pittman Jr C.U., Grunlan, J., Wang Q., Lacy Jr T., Fire impact on mechanically failed graphite/epoxy composites, *Polymer Composites*, **44**(4): 2236–2249, 2023, https://doi.org/10.1002/pc.27239.

3. Nayfeh A.H., The general problem of elastic wave propagation in multilayered anisotropic media, *The Journal of the Acoustical Society of America*, **89**(4): 1521–1531, 1991, https://doi.org/10.1121/1.400988.

4. Nayfeh A.H., The propagation of horizontally polarized shear waves in multilayered anisotropic media, *The Journal of the Acoustical Society of America*, **86**(5): 2007–2012, 1989, https://doi.org/10.1121/1.398580.

5. Datta S.K., Physical ultrasonics of composites, *The Journal of the Acoustical Society of America*, **130**(6): 4170–4171, 2011, https://doi.org/10.1121/1.3655882.

6. Kamal A.M., Gresil M., Giurgiutiu V., Comparative study of several methods for the calculation of ultrasonic guided waves in composites, [in:] *54th AIAA/ASME/ASCE/AHS/ASC Structures, Structural Dynamics, and Materials Conference*, American Institute of Aeronautics and Astronautics, April 8–11, 2013, Boston, MA, 2013, https://doi.org/10.2514/6.2013-1901.

7. Pavlakovic B., Lowe M., Alleyne D., Cawley P., Disperse: A general purpose program for creating dispersion curves, [in:] *Review of Progress in Quantitative Nondestructive Evaluation*, **16**: 185–192, Springer, Boston, MA, 1997, https://doi.org/10.1007/978-1-4615-5947-4_24.

8. Monnier T., Lamb waves-based impact damage monitoring of a stiffened aircraft panel using piezoelectric transducers, *Journal of Intelligent Material Systems and Structures*, **17**(5): 411–421, 2006, https://doi.org/10.1177/1045389X06058630.

9. Azkour M., El Allami M., Rhimini H., Calculation of the dispersion curves modeling the propagation of ultrasonic Lamb waves in a bonded aluminum/epoxy/aluminum structure using the semi-analytical finite element method, *Engineering Transactions*, **72**(2): 119–143, 2024, https://doi.org/10.24423/EngTrans.3171.2024.

10. Yacoubi A., Jabiri A., Azkour M., Mandry R., El Allami M., Wavelet analysis of ultrasonic Lamb wave displacements in three-layer adhesive plates: continuous wavelet transform (CWT) versus the semi-analytical element method (SAFEM), *Engineering Transactions*, **72**(2): 203–224, 2024, https://doi.org/10.24423/EngTrans.3207.2024.

11. Zitouni I., Rhimini H., Chouaf A., Comparative study of the spectral method, DISPERSE and other classical methods for plotting the dispersion curves in anisotropic plates, *Journal of Applied and Computational Mechanics*, **9**(4): 955–973, 2023, https://doi.org/10.22055/jacm.2023.42530.3941.

12. Zitouni I., Rhimini H., Chouaf A., Modeling the propagation of ultrasonic guided waves in a composite plate by a spectral approximation method, *Engineering Transactions*, **71**(2): 213–227, 2023, https://doi.org/10.24423/EngTrans.3073.20230510.

13. Zitouni I., Mekkaoui M., Rhimini H., Chouaf A., Innovative approach to modeling propagative, non-propagative and complex modes of ultrasonic guided waves, *Mechanics of Advanced Materials and Structures*, **32**(8): 1754–1767, 2024, https://doi.org/10.1080/15376494.2024.2370032.

14. Liu H., Huang Z., Yin Z., Sun M., Bo L., Li T., Tian Z., Investigation of viscoelastic guided wave properties in anisotropic laminated composites using a Legendre orthogonal polynomials expansion–assisted viscoelastodynamic model, *Polymers*, **16**(12): 1638, 2024, https://doi.org/10.3390/polym16121638.

15. Bocchini P., Marzani A., Viola E., Graphical user interface for guided acoustic waves, *Journal of Computing in Civil Engineering*, **25**(3): 202–210, 2011, https://doi.org/10.1061/(ASCE)CP.1943-5487.00000.

16. Huber A., The dispersion calculator – a free software for calculating dispersion curves of guided waves, [in:] *20th World Conference on Non-Destructive Testing (WCNDT 2024)*, Incheon, South Korea, 2024, https://doi.org/10.58286/29894.

17. Barski M., Pająk P., Determination of dispersion curves for composite materials with the use of stiffness matrix method, *Acta Mechanica et Automatica*, **11**(2): 121–128, 2017, https://doi.org/10.1515/ama-2017-0019.

18. Zitouni I., Rhimini H., Chouaf A., A combined Newton–bisection approach for calculating the dispersion curves in anisotropic multilayered waveguides, *Journal of Vibration Engineering & Technologies*, **12**(2): 5189–5201, 2024, https://doi.org/10.1007/s42417-023-01191-1.

19. Zitouni I., Rhimini H., Chouaf A., Modeling the propagation of ultrasonic guided waves in four-layer laminated composites, [in:] Azari Z., El Had K., Ait Ali M.E., El Mahi A., Chaari F., Haddar M. [Eds.], *Advances in Applied Mechanics. JET 2022. Lecture Notes in Mechanical Engineering*, Springer, Cham, 2024, https://doi.org/10.1007/978-3-031-49727-8_3.

20. Zitouni I., Rhimini H., Chouaf A., Calculation of dispersion curves in the composite graphite-epoxy plate by a hybrid analytic method, [in:] *Advances in Mechanics. CMM 2022. Lecture Notes in Mechanical Engineering*, Aniss S., *et al.* [Eds.], Springer, Cham, 2024, https://doi.org/10.1007/978-3-031-46973-2_1.

21. Zitouni I., Rhimini H., Chouaf A., Spectral method for modeling the dispersion of complex guided wave modes in anisotropic pipeline, *Journal of Computational Applied Mechanics*, **55**(3): 473–484, 2024, https://doi.org/10.22059/jcamech.2024.376537.1090.

Received December 22, 2024; accepted version January 31, 2025.
Online first April 15, 2025.